Chromium-based covalent coordination nano-polymer: a promising dye elimination compound for water purification

Mojgan Jafari Pirouz[a], Mohammad Hassan Amini[b,*], Mostafa Hossein Beyki[a]

[a]*School of Chemistry, University College of Science, University of Tehran, Tehran, Iran, emails: mhosseinbaki@yahoo.com (M.H. Beyki), mjpirouz@ut.ac.ir (M.J. Pirouz)*
[b]*Chemistry and Chemical Engineering Research Center of Iran, Tehran, Iran, emails: Amini@ccerci.ac.ir/hassanamini4@gmail.com*

ABSTRACT

The goal of this research is to describe a promising dye elimination platform based on covalent coordination framework (CCF) nanoparticles. For this purpose trigonal prismatic molecular building block was prepared by employing 4-hydroxybenzoic acid and Cr(III) salt then the polymerization was performed based on the Mannich reaction using phenylenediamine as a linker. Prepared nanostructure was characterized using Brunauer–Emmett–Teller (BET), field emission scanning electron microscopy (FE-SEM), Fourier-transform infrared spectroscopy, X-ray diffraction (XRD), energy-dispersive X-ray spectroscopy, and elemental mapping techniques. According to the BET results, the nanoparticles showed a surface area of 13.6 m^2 g^{-1}. Moreover, based on the XRD and FE-SEM results the nanoparticles have low crystallinity with a diameter between 15–50 nm. The prepared CCF was employed for the removal of five carcinogenic dyes including; Crystal violet, Malachite green, Methylene blue, Nile blue, and Sunset Yellow. Experimental results showed that maximum removal was obtained at a pH of 9 with a shacking time of 20 min. Kinetic study showed that dye adsorption followed the pseudo-second-order model as well as the dye adsorption behavior followed the Langmuir isotherm model. A 95% desorption of adsorbed dyes was observed with a mixture of 1 mL ethanol and HNO_3 solution with a concentration of 0.1 mol L^{-1}. Moreover, the reusability experiment showed after 3 cycles of sorption and desorption the removal percentage decreased only 5%–10% that confirmed the nano-polymer is a good candidate to be used as a reusable adsorbent for water purification.

Keywords: Covalent coordination framework; Porous material; Dye; Kinetic; Isotherm

1. Introduction

Dyes with a frequency of 100,000 different types; are the main categories of synthetic materials with a critical role in different industries. In recent decades, more than several million tons of dyes are consuming in various industries such as hair colorings, printer paper, textile dyers, plastics, and food technology [1–3]. Despite the wide applicability of dyes, most types of them are categorized as hazardous compounds that cause allergic dermatitis and mutations. Besides, their highly visible displeasing effect causes disturbing the biological phenomena in water ecosystems. The mentioned drawback of dyes convinced the researchers to develop efficient and cost-efficient wastewater treatment techniques to bring the dye value to the permissible limit in water-bodies [4,5]. Up to now, several techniques were developed for dye elimination from water such as; adsorption, oxidation, membrane filtration and

* Corresponding author.

electrochemical process. Among the mentioned techniques adsorption is a promising method regarding toxicological and ecological points [6–10]. One of the main factors in the adsorption process is the adsorbent type which affects the efficiency of the process on a huge level. Among the various type of adsorbents, materials with wide surface area and porous structure are preferred due to offering high adsorption capacity, fast removal efficacy as well as provide adsorption in a selective manner [11–13].

In recent decades several types of porous materials such as zeolites and porous carbons with unique characteristics are synthesized and employed for water purification but some of them have a limited number of specific active sites as well as a highly hydrophobic surface which impedes their practical application [14]. Recently, covalent organic frameworks (COFs) attracted great attention as a new platform for designing advanced organic materials. Since they allow the atomically precise integration of building blocks into periodicities [15,16]. These characteristics make COFs excellent candidates for gas storage [17,18], lithium-sulfur batteries [19], photoelectricity, catalysis and adsorbent [20–22]. Based on the merits of COFs this work represents a new class of two-dimensional porous adsorbent called covalent coordination frameworks (CCFs) synthesized by a two-step approach [23]. The first step includes trigonal prismatic molecular building block formation by using 4-hydroxybenzoic acid and Cr(III) salt. In the second step, the polymerization takes place between the molecular building block and aromatic diamine compound by the formation of strong covalent bonds based on the Mannich reaction. The prepared CCF was employed as a novel adsorbent for the removal of five carcinogenic dyes including; Crystal violet (CV), Malachite green (MG), Methylene blue (MB), Nile blue (NB) and Sunset Yellow (SY). Effective parameters on dye adsorption such as pH, contact time, and adsorbent dosage were optimized moreover, kinetic and isotherm models were studied.

2. Experimental

2.1. Materials and instruments

Cr(NO$_3$)$_3$·9H$_2$O, methanol, 4-hydroxybenzoic acid, and 1,4-phenylenediamines were used to prepare CCF. Dyes were supplied from Merck (Darmstadt, Germany). pH adjustments were performed with HCl and NaOH solutions (0.1 mol L^{-1}).

Several characterization techniques were employed to study the structure of the CCF. Powder X-ray diffraction analysis (XRD) was recorded with Philips powder diffractometer, X'PERT MPD, using Cu-Kα radiation at λ = 1.540589 Å. Field emission scanning electron microscopy (FE-SEM), energy-dispersive X-ray (EDX) and elemental mapping carried out using the SIGMA VP ZEISS instrument. Fourier-transform infrared spectra (FTIR) was measured with Equinox 55 Bruker at the wavenumber of 400–4,000 cm^{-1}. The N$_2$ adsorption–desorption isotherms were recorded on a Nova Station A system. A digital pH-meter (Model 692, Metrohm, Herisau, Switzerland) was used for the pH adjustment. A LAMBDA 25 UV-Vis spectrophotometer was used for recording the light absorption behavior of dyes.

2.2. Synthesis of CCF

To prepare CCF nanoparticles, the first step includes the synthesis of [Cr$_3$(μ$_3$-O)(RCO$_2$)$_6$] molecular building block. In a typical run, 1.3 g of Cr(NO$_3$)$_3$·9H$_2$O was dissolved in 25 mL of methanol by refluxing for 30 min. 1.0 g of hydroxybenzoic acid was dissolved in 25 mL of methanol and added to Cr solution then refluxed for 24 h. In the subsequent step, the solvent was evaporated and a dark green mass was collected [24]. The second step including polymerization based on the Mannich reaction hence 1.0 g of prepared building block was dissolved in 50 mL ethanol followed by the addition of 1.0 g of diamine and 0.3 g of p-formaldehyde. The mixture was refluxed for 24 h and then collected with a centrifuge at 5,000 rpm for 30 min, washed with distilled water, and dried at 60°C for 6 h. The preparation process has been summarized as the below scheme.
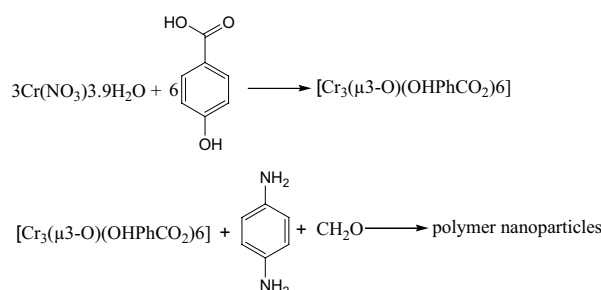

Fig. 1. Preparation process of the polymer nanoparticles.

2.3. Adsorption procedure

The batch equilibrium technique was used to perform dye adsorption experiments at room temperature (293 K). To do so, about 20 mg of CCF nanoparticles were added into 10 mL of dyes solution of known concentration (10–100 mg L^{-1}). After adjustment of pH to 9.0, it was shaken for 20 min to reach the equilibrium. At the end of the adsorption period, the adsorbent was separated from the dye solution by applying a centrifuge (5,000 rpm, 10 min). Finally, the concentration of dyes in the supernatant was determined by measuring the absorbance at the λ$_{max}$ using a UV-Vis spectrophotometer. The amount of dye adsorbed at equilibrium, Q_e (mg g^{-1}), was calculated by the following equation:

$$Q_e = \frac{(C_i - C_e)V}{m} \tag{1}$$

At this equation, C_i and C_e (mg L^{-1}) are equal to initial and equilibrium concentrations of dyes, respectively. The V (L) is the volume of the aqueous solution, and m (g) is the weight of the CCF nanoparticles.

3. Results and discussion

3.1. Characterization of the CCF

The elemental composition of the CCF nanoparticles was analyzed by elemental mapping and EDX techniques and the results are shown in Fig. 2. It can be seen from Fig. 2a that carbon, nitrogen, oxygen and chromium are
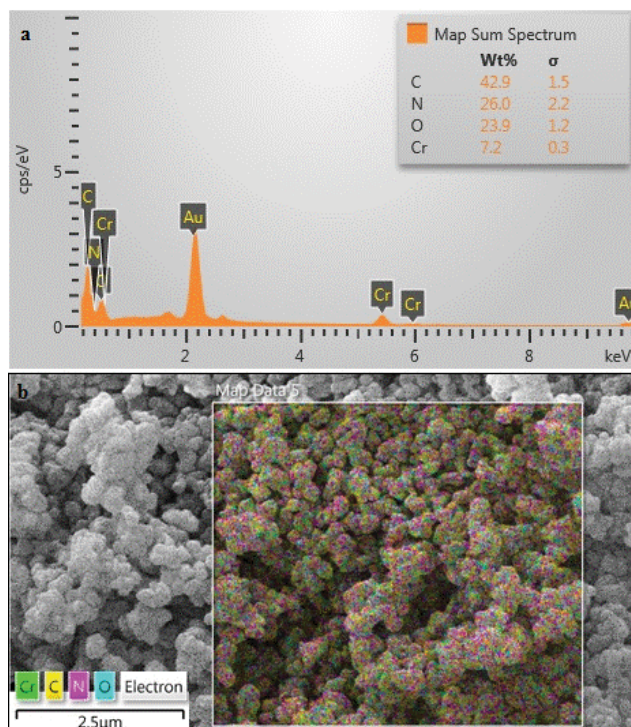
Fig. 2. EDX spectrum (a) and elemental mapping (b) of the CCF.

Fig. 3. XRD pattern of the CCF.

Fig. 4. FTIR spectra of the CCF.

the main components of the CCF which are corresponding to employed starting materials. Carbon with a frequency of 42.9% that is originated from the phenylenediamine and hydroxybenzoic acid is the main component of CCF. Other components of nanoparticles are present in the CCF structure with good density. Fig. 2b showed the mapping of the CCF nanoparticles. It can be seen that the elements are uniformly distributed in the CCF structure.

The crystallinity of the CCF nanoparticles was confirmed with the XRD analysis and the pattern is illustrated in Fig. 3. The pattern shows a main sharp reflection at a low 2θ value of 8.6° attributed to the (001) plan. A clear low intense peak at 2θ value of 24.3° is also observable which is corresponding to 111 reflections of the CCF. The observed reflections could be indexed to a pseudo-orthorhombic cell [25]. The peak at 2θ = 24.3° is equal to periodicity perpendicular to the polymer chain. It also can be attributed to the distance between the benzene rings in adjacent chains or the close contact inter-chain distance [26]. According to the angle of the first peak at 8.6°, the interlayer d-spacing of the CCF is equal to 10.23 Å.

The CCF structure contains several functional groups including C=O, OH, NH, CH and benzenoid ring. FTIR spectra were employed for detecting the functional groups of the CCF. The spectrum is shown in Fig. 4. The spectrum shows a broad peak at 3,000–3,400 cm^{-1}. This district of FTIR is corresponding to hydroxyl and NH groups which can be attributed to the stretching vibration of them. Moreover, the C=O vibration with high intensity appeared at 1,600 cm^{-1}. A peak with high intensity at 1,374 cm^{-1} corresponds to the OH bending vibration of phenolic groups [27,28]. Stretching vibration at around 1,500 cm^{-1}
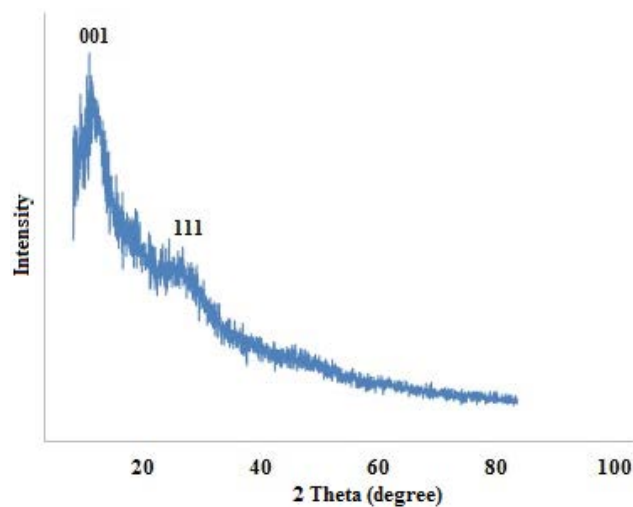
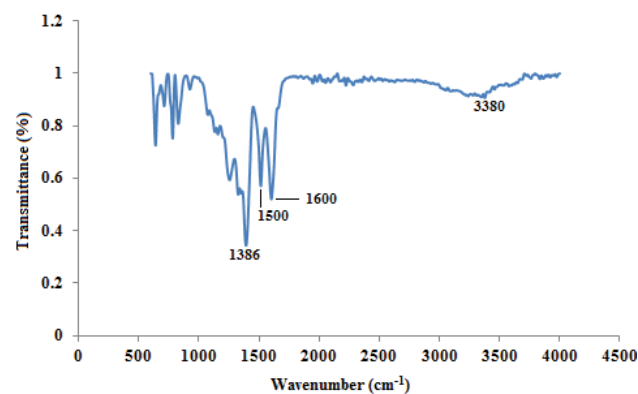corresponds to (C=C) that can be attributed to the benzenoid ring.

The porosity of the CCF is studied with the N_2 adsorption–desorption isotherm. Results are depicted in Fig. 5a. It can be seen that the N_2 adsorption–desorption isotherm show some hysteresis loop. The loop appearing is owed to the filling and emptying of the mesopores by capillary condensation. The isotherm belongs to type II with a subset of B which confirms the pores have a slit shape with a parallel wall [29]. Moreover, the pore-size distribution curve of the CCF is shown in Fig. 5b with an average pore size of 2.0 nm. The specific surface area and pore volume for the particles were 13.6 m^2 g^{-1} and 0.018 cm^3 g^{-1}, respectively. According to the results, the CCF is a mesoporous compound owed to the defects between the components.

The morphology of the CCF was studied with the FE-SEM technique and the image displayed in Fig. 6. It can be seen that discrete particles are not clear. The image showed aggregated structures that were built of accumulated particles with a diameter between 15–50 nm. The structure of the CCF is composed of hydroxyl and amine groups which interact with each other through hydrogen bonding and cause aggregation between the particles. Moreover,
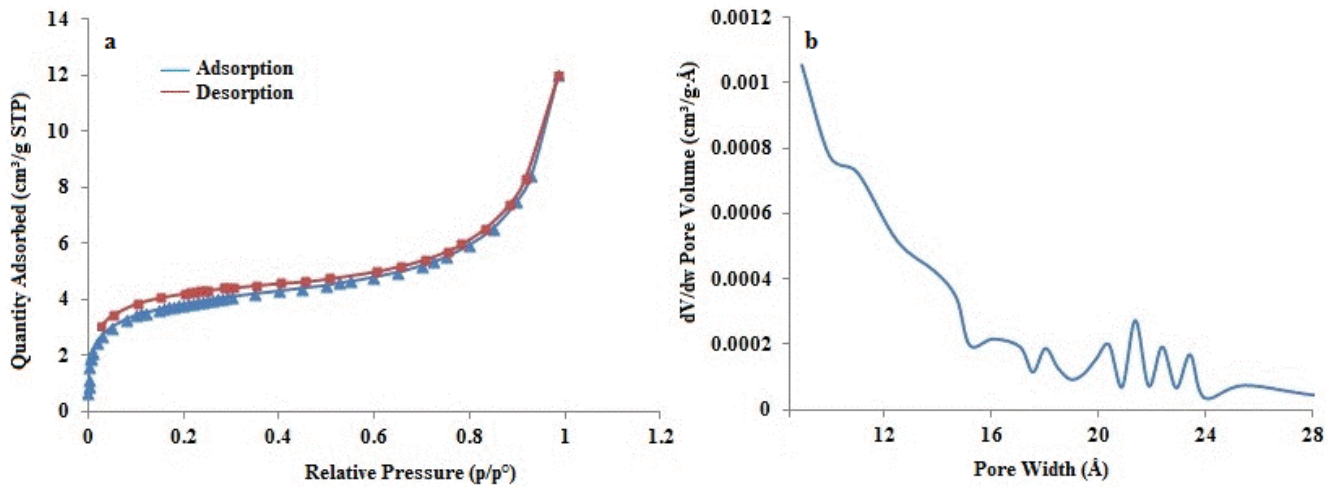
Fig. 5. N$_2$ adsorption–desorption curve (a) and pore size distribution (b) of the CCF.
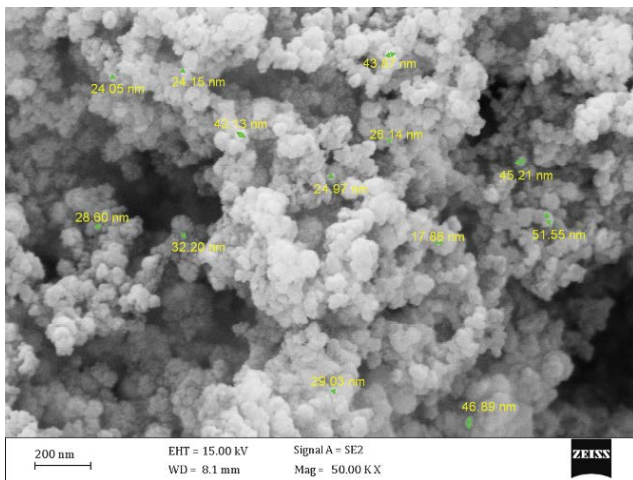

Fig. 6. FE-SEM image of the CCF.

hydrophobic interactions among the aromatic backbones induce agglomeration of the CCF nanoparticles.

3.2. Adsorption experiments of carcinogenic dyes over CCF nanoparticles

There are several variables affecting dye adsorption efficiency which are important factors in the water treatment process. The optimization of variables such as contact time, solution pH, temperature, and initial dye concentration can help the development of industrial-scale dye removal. In other words, performing dye removal process at the optimum conditions makes the process more efficient and economic. Solution pH was selected as the first variable to be optimized since, in aqueous media, surface properties of the sorbent, as well as the chemistry of the functional groups of dye, are affected by the pH of the solution hence, the efficiency of the adsorption process is primarily affected by this parameter. The second studied factor in the adsorption process is the amount of adsorbent or adsorbent dosage that can

maximize or minimize the adsorption efficacy through changing analyte–sorbent interactions. Removal efficiency may be lower than the real value at an insufficient value of adsorbent dosage, besides at a high level of adsorbent screening effect may occur at the outer layer of the sorbent particles that hinder the binding sites from the target analyte [30]. Solution temperature is another factor that can increase or decrease the removal efficiency if the process is endothermic or exothermic, respectively. Another variable is initial dye concentration that may increase or decrease the efficiency based on the adsorption mechanism, that is, multilayer or monolayer process. For optimizing the parameters dyes concentration was constant at 10 mg L^{-1} to avoid further dilution of the supernatant since the dye concentration should be in the linear range of the UV-Vis spectrophotometer. Contact time is the final variable that has been described since based on the experimental results this factor has a moderate effect on the removal percentage.

3.2.1. Effect of pH

To evaluate the effect of the pH on dyes adsorption efficiency, several experiments were implemented in the pH range of 2.0–9.0 at the constant value of other variables (adsorbent amount of 20 mg and 30 min shacking time). For this purpose, a series of dye solutions with a volume of 10 mL and dyes concentration of 10 mg L^{-1} was prepared and after adding the adsorbent, was shacked for 30 min. Afterward, the sorbent was separated with centrifugation, and removal percentage was calculated using Eq. (2), where C_0 and C_e are the initial and equilibrium concentrations (mg L^{-1}) of dyes in the solution.

$$R\% = \frac{(C_0 - C_e)}{C_0} \times 100 \tag{2}$$

According to the results in Fig. 7, dye removal percentage is increased with an increase in working pH and reached a maximum level at alkaline solutions, that is, the pH of 9. This can be described based on the dyes structural
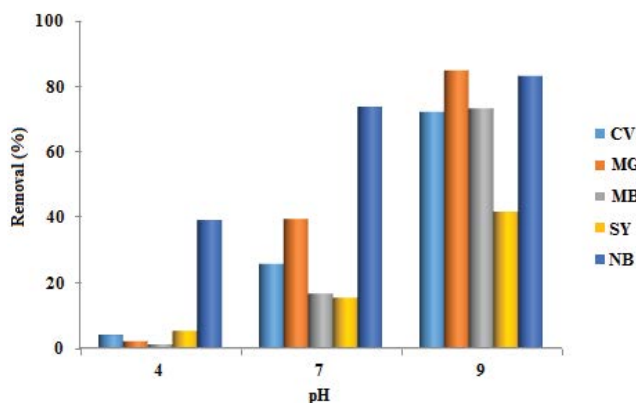
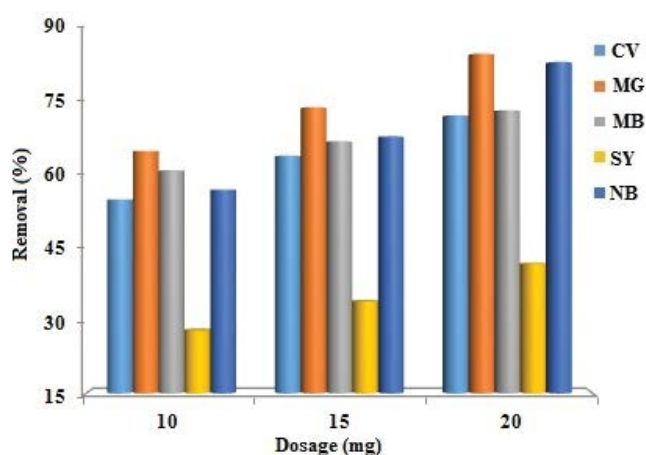Fig. 7. Effect of solution pH on dye adsorption removal.

Fig. 8. Results of adsorbent dosage effect on the adsorption of the dyes.

Fig. 9. Effect of temperature on the adsorption of dyes by the polymer nanoparticles.

charge and surface charge of the adsorbent. In other words, the most selected dyes are cationic types (SY is anionic dye) that have a positive electrical charge in their structure. Besides increasing the pH of the solution, the hydroxyl functional group of the CCF is predicted to exist predominantly in a deprotonated form with a negative charge. Hence, the electrostatic attraction between cationic dyes and the sorbent surface is the main reason for the high removal efficiency of dyes from alkali solution [31]. Besides, the sorbent surface contains several H-bonding sites including; NH and OH groups which interact with the polar organic dyes through hydrogen bonding reaction. Among the employed dyes SY is an anionic dye but it also obeyed the adsorption manner of cationic dyes with the change of pH, that is, its adsorption increased with an increase in pH. This manner can be explained by the π–π bond formation between aromatic backbones of the dye and CCF. In other words; the functional groups of the sorbent and SY could be considered as either electron-donors or acceptors and the tendency of them to accept or donate electrons also determines the strength of the π–π bond. At the working pH, the hydroxyl groups of the dye and the sorbent are in a deprotonated form that increases the density of electrons in their structure as a result increases the π–π binding ability of them [32].

3.2.2. Effect of adsorbent dosage

The effect of adsorbent dosage was examined at three levels of 10, 15 and 20 mg of the CCF and the results depicted in Fig. 8. It was observed that the removal efficiency enhanced greatly with an increase in the adsorbent dosage. This situation is owed to the increase in the density of the surface-active group as a result; they can capture more value of dye molecules. In other words, to obtain higher removal efficiency, 20 mg was selected as the optimum adsorbent dosage.

3.2.3. Effect of temperature

Effect of temperature on dyes adsorption has been examined on 10 mL sample solution with a concentration of 10 mg L^{-1} at 293, 313 and, 333 K. The result in Fig. 9 showed that dyes adsorption on the nano-polymer increased with the increase of temperature. This suggests that the adsorption is an endothermic process and the adsorption
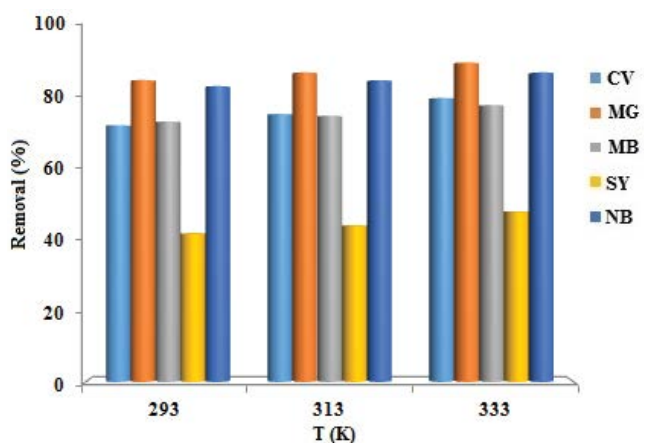
was feasible at high temperature. This situation may be owing to the increase in the mobility of dyes molecules with the temperature that increases the diffusion rate of the molecules through the external boundary layer and the internal pores of the adsorbent particles [33]. It can be seen that increase in the removal percentage is not significant as with the increase of temperature from 293 to 333 K the removal percentage increased about 4%–8%. Based on the results it can be concluded that adsorption of the dyes by the adsorbent at high temperature is not economic therefore room temperature (293 K) has been selected for further work.

3.2.4. Effect of initial dye concentration

Results of the effect of initial dyes concentration in the range of 10–100 mg L^{-1} on removal percentage are presented in Fig. 10. It can be seen that the sorption of MG and NB is 83% and 85% at an initial concentration of 10 mg L^{-1}. The removal efficiencies of CV, MB and SY are 72%, 43% and 41%, respectively. At higher initial concentration, the efficiency is decreased so that at an initial concentration of 100 mg L^{-1} the removal percentage of CV, MG, MB, SY
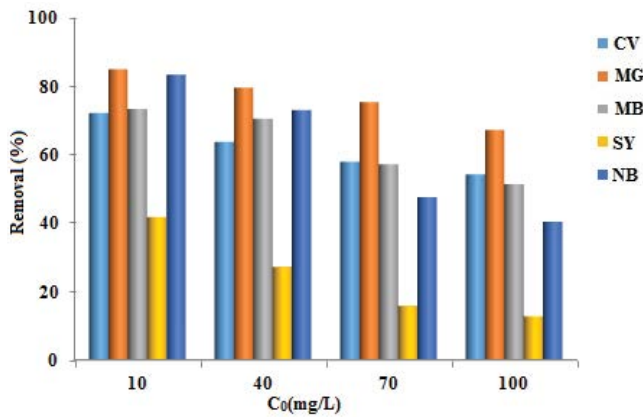
Fig. 10. Effect of initial dyes concentration on the removal efficiency.

Fig. 11. Effect of contact time on dye removal by the CCF.

and NB is 54%, 67%, 51%, 12% and 40%, respectively. The observed results can be explained based on the fact that the structure of the adsorbent possesses a certain number of active functional groups that react with the dyes molecules. After the occupation of the sites with dyes, accessible active sites are at a low level hence the removal efficiency decreases.

3.2.5. Effect of contact time and kinetic study

Effect of contact time on dyes adsorption was performed within 1–30 min using 10 mL of the dyes solution with the concentration of 10 mg L^{-1}. Results are depicted in Fig. 11. It can be seen that the adsorption process followed the same uptake pattern at the mentioned experimental conditions; in other words, it can be seen that removal percentage is increased smoothly with the increase in time and then, it is slowed down as the sites are gradually filled up. The first fast removal within 1 min is due to the availability of a large number of adsorption sites or the external electrostatic adsorption in the absence of internal diffusion. At higher interaction times the kinetics will be dependent on the rate of dyes transport from the liquid phase to the CCF surface. The increase in removal efficiency is not significant after 30 min hence this time is selected for further work.

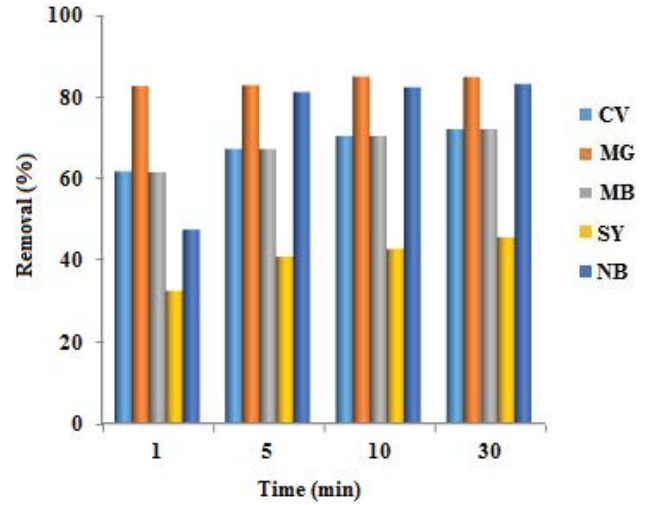The kinetic of dyes adsorption onto CCF was further investigated based on the pseudo-first-order and pseudo-second-order models. These models can be described with the following linear equations, where K_1 and K_2 are the pseudo-first-order rate constant (min^{-1}) and pseudo-second-order rate constant of sorption (g mg^{-1} min^{-1}). Moreover, Q_e and Q_t represent the amount of analyte adsorbed at time t and equilibrium (mg g^{-1}), respectively [34–36].

$$\ln\left(Q_e - Q_t\right) = \ln Q_e - K_1 t \tag{3}$$

$$\frac{t}{Q_t} = \frac{t}{Q_e} + \frac{1}{K_2 Q_e^2} \tag{4}$$

The values of the kinetic parameters are listed in Table 1. It can be seen that the second-order model possesses high linearity with the same R^2 values for all dyes. The high R^2 values (0.99) for pseudo-second-order expression suggest that this model may be appropriate to use for describing the kinetic adsorption properties of the sorbent. Moreover, the results showed that the Q_e obtained based on the pseudo-second-order model, has a lower deviation from experimental values compared with that achieved with the first-order model as a result the pseudo-second-order model can better describe the kinetic behavior of dyes adsorption by CCF.

Table 1
Data of kinetic models for the adsorption of dyes using CCF (adsorbent: 20 mg; pH = 9; sample volume: 10 mL)

		CV	MG	MB	SY	NB
First-order	R^2	0.99	0.83	0.99	0.88	0.86
	K_1 (min^{-1})	0.19	0.47	0.19	0.23	0.39
	Q_e (mg g^{-1})	0.63	0.37	0.63	1.19	3.32
Second-order	R^2	0.99	0.99	0.99	0.99	0.99
	K_2 (g mg^{-1} min^{-1})	0.88	3.33	0.86	0.36	0.19
	Q_e (mg g^{-1})	3.66	4.34	3.7	2.43	9.09
	Q_{exp} (mg g^{-1})	5.54	4.25	3.61	2.28	8.33

3.2.6. Isotherm study and error analysis

The Langmuir and Freundlich isotherm models are used to further analysis of the effect of dyes concentration on the sorption process. These models are expressed by the following linearized equations, where Q_e is the amount of analyte adsorbed per unit mass of the sorbent (mg g^{-1}) and C_e is the amount of analyte in the liquid phase at equilibrium (mg L^{-1}). The Q_m is the maximum adsorption capacity, b is Langmuir constant and K_f and n, are Freundlich coefficients [37,38].

$$\frac{C_e}{Q_e} = \frac{1}{Q_m b} + \frac{C_e}{Q_m} \tag{5}$$

$$\log Q_e = \log K_f + \frac{1}{n} \log C_e \tag{6}$$

The data equal to the Langmuir and Freundlich isotherm models are shown in Table 2. Based on the results, the data for dyes adsorption (except CV) exhibited the best fit to the Langmuir model since they exhibit relatively higher R^2 values in comparison with the Freundlich model. However, the Freundlich model also shows approximately good linearity but the linearity is lower than those of the Langmuir model hence it may be concluded that the adsorption process does not follow the Freundlich model. The accuracy of the suggestion is further studied with the sum of the squared residual (RSS). This error function is given as Eq. (7), where Q_{exp} and Q_c are the experimental and calculated data from nonlinear models [39].

$$\text{RSS} = \sum \left(Q_c - Q_{exp} \right)^2 \tag{7}$$

Based on the results presented in Table 2, the Langmuir model has lower RSS values that revealed the Langmuir model can better describe the adsorption behavior of dyes on the CCF.

3.3. Adsorption mechanism

The adsorption process may be occurring through a chemical or physical route. These phenomena can understand using the results of kinetic and isotherm studies. The second-order kinetic model is equal to chemisorption besides; the first-order kinetic model represents physical adsorption or ion exchange. Moreover, the Freundlich isotherm model explains multilayer adsorption while the Langmuir model shows a monolayer chemisorption process [40]. According to the experimental results, dyes adsorption onto CCF followed Langmuir isotherm model and second-order kinetic model hence it can be concluded that chemisorption is the dominant mechanism of dyes adsorption; however, physical adsorptions could not be discarded thoroughly. As a result, it can be concluded that multiple mechanisms acted simultaneously in dye adsorption. The chemical structure of the CCF and three types of dyes are depicted in Fig. 12. It can be seen that the CCF structure contains several non-polar fragments including the benzenoid ring and methylene groups.

Table 2
Data of Langmuir and Freundlich isotherm models for the adsorption of dyes using CCF (adsorbent: 20 mg; pH = 9; sample volume: 10 mL)

Model	Constant	CV	MG	MB	SY	NB
Langmuir	Q_m (mg g^{-1})	47.6	52.63	38.46	7.14	45.45
	b (L mg^{-1})	0.027	0.057	0.043	0.077	0.068
	R^2	0.97	0.99	0.98	0.98	0.98
	RSS	0.75	0.75	3.16	0.37	18.02
Freundlich	K_f (mg$^{1-1/n}$ g^{-1}) (L)$^{1/n}$	1.73	3.38	2.33	1.09	5.62
	n	1.38	1.45	1.51	2.43	2.32
	R^2	0.99	0.98	0.96	0.92	0.91
	RSS	0.31	9.59	7.18	1.21	56.28

Therefore, hydrophobic interaction between dyes and the surface of the sorbent is one of the probable dye uptake mechanisms by the CCF. The structure of CCF and dyes also contains polar functional groups, that is, oxy/hydroxy and amine groups. Hence it can be concluded that hydrogen bonds also participate in dye adsorption. Based on the effect of solution pH on the adsorption efficiency it seems that the main way for dye adsorption onto CCF nanoparticles is electrostatic attraction since most employed analytes are cationic dyes which can be adsorbed on the sorbent surface through interaction with the negatively charged sorbent [41,42]. This conclusion is based on the zeta potential measurements in Fig. 13. It can be seen that the adsorbent surface has a negative charge above pH of 4 as reached to high negative charge at a pH of 9.

3.4. Desorption and reusability

From a practical point of view, to make the sorption process more economic, desorbs of the target analyte from the sorbent surface are necessary. According to results for the effect of pH, the adsorption of dyes was not efficient in the acidic mediums hence elution with acidic solution may be favorable. Moreover, it can be estimated that the employment of an organic solvent is a good choice to release the adsorbed dyes. As a result, different concentration of HNO$_3$ solution (0.01, 0.05 and 0.1 mol L^{-1}) and 1 mL of ethanol was employed to reuse the adsorbent. It was observed that in the mixture of 1 mL ethanol and HNO$_3$ solution with a concentration of 0.1 mol L^{-1}, the release of dyes was more than 95%. Moreover, to evaluate the reusability of the sorbent, it was subjected to several loadings with the sample solution and subsequent elution. It was found that after 3 cycles of sorption and desorption (Fig. 14), the removal percentage decreased about 5%–10%. Results confirmed that the nano-polymer is a good candidate to be used as a reusable adsorbent for water purification.

3.5. Comparing with other methods

To evaluate the efficacy of the presented work for dye removal the performance of CCF was compared with previously used adsorbents for removal of dyes. Three
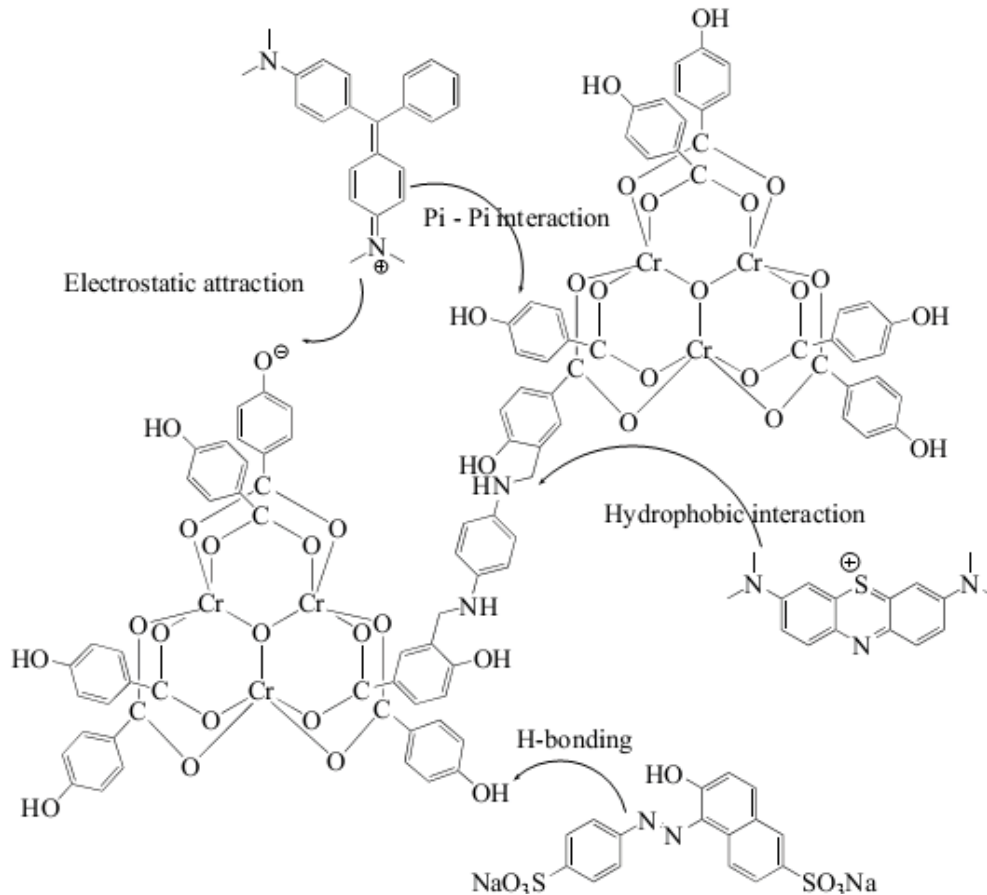
Fig. 12. Schematic illustration of dyes adsorption onto the CCF surface.

Table 3
Comparison of dyes adsorption onto CCF with different adsorbents

Adsorbent	Dyes removed	Q_{max} (mg g^{-1})	Time (min)	Dosage (mg)	References
NiFe$_2$O$_4$ – activated carbon	Direct red 31, Direct blue 78	299.67, 209.13	25	20	[1]
Exfoliated graphite	Methylene blue, Rhodamine B	90, 15	5 s	1	[2]
Aspergillus niger biomass	Acid yellow 99	544.30	245	20	[4]
Thiourea – chitosan	Congo red	44.248	200	100	[5]
Sodium alginate/silicon dioxide	Methylene blue	148.23	150	200	[7]
Zn–Al–NO$_3$-LDH	Evans blue	113.64	120	25	[8]
Polymer	Remazol Brilliant Blue R	238.10	59.91	40	[12]
COF-2D NPs	Eosin, fluorescein	55.34, 26.58	170	100	[22]
CoFe$_2$O$_4$	Remazol Red RB-133 dye	41.7	180	50	[33]
Chromium based CCF	Crystal violet, Malachite green, Methylene blue, Nile blue, Sunset yellow	47.6, 52.63, 38.46, 7.14, 45.45	30	20	This work

adsorption parameters including adsorbent dosage, adsorption capacity and contact time was selected for comparison and results are shown at Table 3. It can be seen that adsorption process on CCF is faster than the must reported adsorbents along with lower adsorbent dosage for the dyes removal. Moreover, the adsorption capacity of target dyes on this adsorbent is in good level as it is in same level in comparing with COF nanoparticles [22]. In summary, proposed nano-polymer showed desired properties such as; fast adsorption rate, low adsorbent dosage, ease of regeneration and reuse as well as applicability for removal of both anionic and cationic dye.
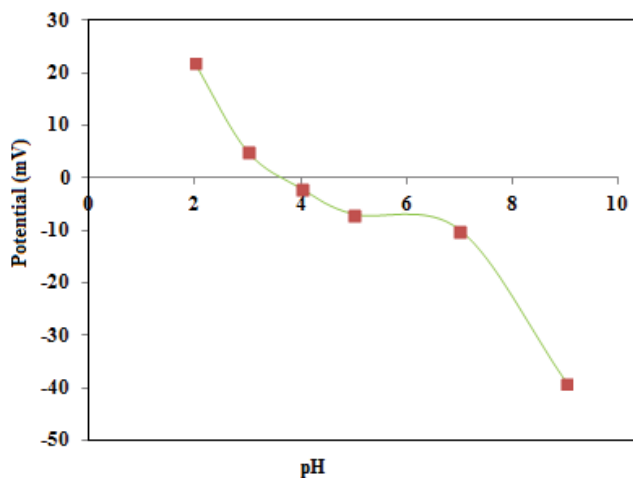
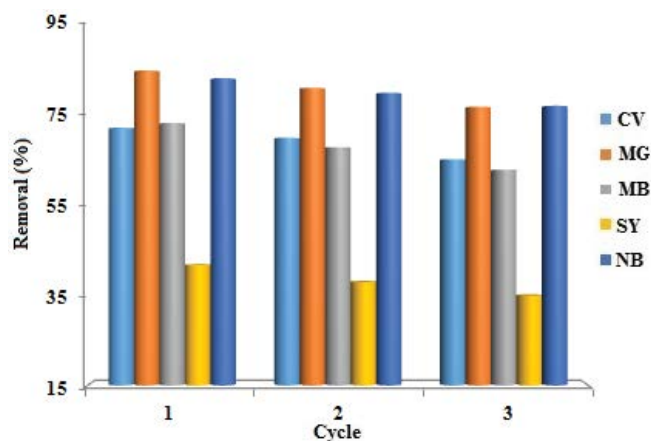Fig. 13. Zeta potential measurements of the polymer nanoparticles.

Fig. 14. Reusability results of the adsorbent after three cycles of sorption and desorption.

4. Conclusions

The coordination covalent framework nanoparticles were synthesized by the crosslinking polymerization of chromium-based molecular building blocks and diamine monomer. Characterization techniques, that is, FTIR, SEM, EDX, Brunauer–Emmett–Teller and XRD were used to confirm the formation of the CCF nanoparticles. It was found that the nanoparticles diameter is about 15–50 nm with a surface area of 13.6 m^2 g^{-1}. The prepared nanoparticles were employed for the removal of carcinogenic dyes from aqueous solutions. Maximum removal was obtained at pH = 9 within 20 min. Kinetic study showed the adsorption process followed the pseudo-second-order model. Isotherm's study revealed that the Langmuir model can better describe the adsorption process. Desorption of adsorbed dyes from the sorbent surface was performed with a mixture of ethanol – HNO$_3$ solution as the release of dyes was more than 95%. Reusability study showed that after 3 cycles of sorption and desorption the removal percentage decreased about 5%–10%. Conclusively, the synthesized nanostructure might be a promising adsorbent for the removal of dyes in dye-contaminated water with good performances.

References

[1] M.J. Livani, M. Ghorbani, Fabrication of NiFe$_2$O$_4$ magnetic nanoparticles loaded on activated carbon as novel nanoadsorbent for Direct Red 31 and Direct Blue 78 adsorption, Environ. Technol. 3330 (2017) 1–17.

[2] J. Mohanraj, D. Durgalakshmi, S. Balakumar, P. Aruna, S. Ganesan, S. Rajendran, Mu. Naushad, Low cost and quick time absorption of organic dye pollutants under ambient condition using partially exfoliated graphite, J. Water Process Eng., 34 (2020) 101078, doi: 10.1016/j.jwpe.2019.101078.

[3] R. Kaveh, H. Alijani, M. Hossein, M. Jafari, Adsorption and oxidation of dye and tetracycline over hydrothermally synthesized polyresorcinol – ferrite nanoparticles, Desal. Water Treat., 212 (2021) 376–389.

[4] A. Naskar, R. Majumder, Understanding the adsorption behaviour of acid yellow 99 on *Aspergillus niger* biomass, J. Mol. Liq., 242 (2017) 892–899.

[5] N.F. El-Harby, S.M.A. Ibrahim, N.A. Mohamed, Adsorption of Congo red dye onto antimicrobial terephthaloyl thiourea cross-linked chitosan hydrogels, Water Sci. Technol., 76 (2017) 2719–2732.

[6] K.-W. Jung, B.H. Choi, M.-J. Hwang, J.-W. Choi, S.-H. Lee, J.-S. Chang, K.-H. Ahn, Adsorptive removal of anionic azo dye from aqueous solution using activated carbon derived from extracted coffee residues, J. Cleaner Prod., 166 (2017) 360–368.

[7] H. Hosseinzadeh, K. Abdi, Efficient removal of methylene blue using a hybrid organic–inorganic hydrogel nanocomposite adsorbent based on sodium alginate–silicone dioxide, J. Inorg. Organomet. Polym. Mater., 27 (2017) 1595–1612.

[8] M. Shamim, K. Dana, Efficient removal of Evans blue dye by Zn–Al–NO$_3$ layered double hydroxide, Int. J. Environ. Sci. Technol., 15 (2017) 1275–1284.

[9] A. Zuorro, G. Maffei, R. Lavecchia, Kinetic modeling of azo dye adsorption on non-living cells of *Nannochloropsis oceanica*, J. Environ. Chem Eng., 5 (2017) 4121–4127.

[10] M. Schwarze, D. Seo, B. Bibouche, R. Schomäcker, Comparison of positively charged polymer species and cationic surfactants for methyl orange removal via polyelectrolyte and micellar enhanced ultrafiltration, J. Water Process Eng., 36 (2020) 101287, doi :10.1016/j.jwpe.2020.101287.

[11] D.D. Sewu, P. Boakye, H. Jung, S.H. Woo, Synergistic dye adsorption by biochar from co-pyrolysis of spent mushroom substrate and *Saccharina japonica*, Bioresour. Technol., 244 (2017) 1142–1149.

[12] G. Torgut, M. Tanyol, F. Biryan, G. Pihtili, K. Demirelli, Application of response surface methodology for optimization of Remazol Brilliant Blue R removal onto a novel polymeric adsorbent, J. Taiwan Inst. Chem. Eng., 80 (2017) 406–414.

[13] L. Ma, G. Zhao, Y. Fang, W. Dai, N. Ma, Facile synthesis of mesoporous calcium carbonate particles with finger citron residue as template and their adsorption performances for Congo red, Adv. Sci. Technol., 36 (2018) 872–887.

[14] J. Wei, D. Zhou, Z. Sun, Y. Deng, Y. Xia, D. Zhao, A controllable synthesis of rich nitrogen-doped ordered mesoporous carbon for CO$_2$ capture and supercapacitors, Adv. Funct. Mater., 23 (2013) 2322–2328.

[15] H. Furukawa, O.M. Yaghi, Storage of hydrogen, methane, and carbon dioxide in highly porous covalent organic frameworks for clean energy applications, J. Am. Chem. Soc., 131 (2009) 8875–8883.

[16] N. Huang, X. Chen, R. Krishna, D. Jiang, Two-dimensional covalent organic frameworks for carbon dioxide capture through channel-wall functionalization, Angew. Chem. Int. Ed., 54 (2015) 2986–2990.

[17] S.S. Han, H. Furukawa, O.M. Yaghi, W.A. Goddard, Covalent organic frameworks as exceptional hydrogen storage materials, J. Am. Chem Soc., 130 (2008) 11580–11581.

[18] Z. Li, Y. Zhi, X. Feng, X. Ding, Y. Zou, X. Liu, Y. Mu, An azine-linked covalent organic framework: synthesis, characterization and efficient gas storage, Chem. Eur. J., 21 (2015) 12079–12084.

[19] Z.A. Ghazi, L. Zhu, H. Wang, A. Naeem, A.M. Khattak, B. Liang, N.A. Khan, Z. Wei, L. Li, Z. Tang, Efficient polysulfide chemisorption in covalent organic frameworks for high-performance lithium-sulfur batteries, Adv. Eng. Mater., 6 (2016) 1–6.

[20] S.-Y. Ding, W. Wang, Covalent organic frameworks (COFs): from design to applications, Chem. Soc. Rev., 42 (2013) 548–568.

[21] S. Dalapati, E. Jin, M. Addicoat, T. Heine, D. Jiang, Highly emissive covalent organic frameworks, J. Am. Chem. Soc., 138 (2016) 5797–5800.

[22] A.R. Abdellah, H. Nasser, A.A.A.M. El-Adasy, A.A. Atalla, K.I. Aly, One-pot synthesis of hierarchical porous covalent organic frameworks and two-dimensional nanomaterials for selective removal of anionic dyes, J. Environ.Chem. Eng., 8 (2020) 104054–104062.

[23] S.K. Elsaidi, M.H. Mohamed, J.S. Loring, B.P. McGrail, P.K. Thallapally, Coordination covalent frameworks: a new route for synthesis and expansion of functional porous materials, ACS Appl. Mater. Interfaces, 8 (2016) 28424–28427.

[24] S.K. Elsaidi, M.H. Mohamed, L. Wojtas, A.J. Cairns, M. Eddaoudi, M.J. Zaworotko, Two-step crystal engineering of porous nets from $[Cr_3(\mu_3\text{-}O)(RCO_2)_6]$ and $[Cu_3(\mu_3\text{-}Cl)(RNH_2)_6Cl_6]$ molecular building blocks, Chem. Commun., 49 (2013) 8154–8156.

[25] J.P. Pouget, M.E. Jozefowicz, A.J. Epstein, X. Tang, A.G. MacDiarmid, X-ray structure of polyaniline, Macromolecules, 24 (1991) 779–789.

[26] J.P. Pouget, C.-H. Hsu, A.G. Mac Diarmid, A.J. Epstein, Structural investigation of metallic PAN-CSA and some of its derivatives, Synth. Met., 69 (1995) 119–120.

[27] Y. Cai, L. Zheng, Z. Fang, Selective adsorption of Cu(II) from an aqueous solution by ion imprinted magnetic chitosan microspheres prepared from steel pickling waste liquor, RSC Adv., 5 (2015) 97435–97445.

[28] S. Liang, X. Guo, N. Feng, Q. Tian, Application of orange peel xanthate for the adsorption of Pb^{2+} from aqueous solutions, J. Hazard. Mater., 170 (2009) 425–429.

[29] H. Yadaei, M.H. Beyki, F. Shemirani, S. Nouroozi, Ferrofluid mediated chitosan@mesoporous carbon nanohybrid for green adsorption/preconcentration of toxic Cd(II): modeling, kinetic and isotherm study, React. Funct. Polym., 122 (2018) 85–97.

[30] N. Tumin, A. Chuah, Adsorption of copper from aqueous solution by Elais Guineensis kernel activated carbon, J. Eng. Sci. Technol., 3 (2008) 180–189.

[31] M.H. Beyki, M. Bayat, F. Shemirani, Fabrication of core-shell structured magnetic nanocellulose base polymeric ionic liquid for effective biosorption of Congo red dye, Bioresour. Technol., 218 (2016) 326–334.

[32] M.H. Beyki, F. Feizi, F. Shemirani, Melamine-based dendronized magnetic polymer in the adsorption of Pb(II) and preconcentration of rhodamine B, React. Funct. Polym., 103 (2016) 81–91.

[33] A.A. Badawy, S.M. Ibrahim, H.A. Essawy, Enhancing the textile dye removal from aqueous solution using cobalt ferrite nanoparticles prepared in presence of fulvic acid, J. Inorg. Organomet. Polym. Mater., 30 (2020) 1798–1813.

[34] C.T. Weber, E.L. Foletto, L. Meili, Removal of tannery dye from aqueous solution using papaya seed as an efficient natural biosorbent, Water Air Soil Pollut., 224 (2013) 1427, doi: 10.1007/s11270–012–1427–7.

[35] C.-H. Wu, Adsorption of reactive dye onto carbon nanotubes: equilibrium, kinetics and thermodynamics, J. Hazard. Mater., 144 (2007) 93–100.

[36] R. Zhao, Y. Wang, X. Li, B. Sun, Z. Jiang, C. Wang, Water-insoluble sericin/β-cyclodextrin/PVA composite electrospun nanofibers as effective adsorbents towards methylene blue, Colloids Surf., B, 136 (2015) 375–382.

[37] A. Buntic, M. Pavlovic, K. Mihajlovski, M. Randjelovic, N. Rajic, D. Antonovic, S. Siler-Marinkovic, S. Dimitrijevic-Brankovic, Removal of a cationic dye from aqueous solution by microwave activated clinoptilolite – response surface methodology approach, Water Air Soil Pollut., 225 (2014) 1816–1829.

[38] Y. Yao, F. Xu, M. Chen, Z. Xu, Z. Zhu, Adsorption behavior of methylene blue on carbon nanotubes, Bioresour. Technol., 101 (2010) 3040–3046.

[39] M.H. Beyki, F. Shemirani, Dual application of facilely synthesized Fe_3O_4 nanoparticles: fast reduction of nitro compound and preparation of magnetic polyphenylthiourea nanocomposite for efficient adsorption of lead ions, RSC Adv., 5 (2015) 22224–22233.

[40] R. Khani, S. Sobhani, M.H. Beyki, S. Miri, Application of magnetic ionomer for development of very fast and highly efficient uptake of triazo dye Direct Blue 71 form different water samples, Ecotoxicol. Environ. Saf., 150 (2018) 54–61.

[41] M.T. Yagub, T.K. Sen, H.M. Ang, Equilibrium, kinetics, and thermodynamics of methylene blue adsorption by pine tree leaves, Water Air Soil Pollut., 223 (2012) 5267–5282.

[42] S.M. Ibrahim, H.M. Hassanin, M.M. Abdelrazek, Synthesis, and characterization of chitosan bearing pyranoquinolinone moiety for textile dye adsorption from wastewater, Water Sci. Technol., 81 (2020) 421–435.